Catalysis Letters (2021) 151:1578–1591
https://doi.org/10.1007/s10562-020-03420-8

Nickel–Promoted Molybdenum or Tungsten Carbides as Catalysts in Dry Reforming of Methane: Effects of Variation in CH_4/CO_2 Molar Ratio

Renato Dias Barbosa[1] · Maria Auxiliadora Scaramelo Baldanza[1] · Neuman Solange de Resende[1] · Fabio Barboza Passos[2] · Victor Luis dos Santos Teixeira da Silva[1]

Received: 2 June 2020 / Accepted: 5 October 2020 / Published online: 12 October 2020

Abstract
Ni–Mo_2C and Ni–WC were evaluated in dry reforming of methane employing different CH_4/CO_2 ratios. Ni–Mo_2C remained active under an excess of CH_4, but deactivation occurred under an excess of CO_2. Ni–WC was resistant to excess of CO_2 but showed carbon deposition under excess of CH_4.

Graphic Abstract

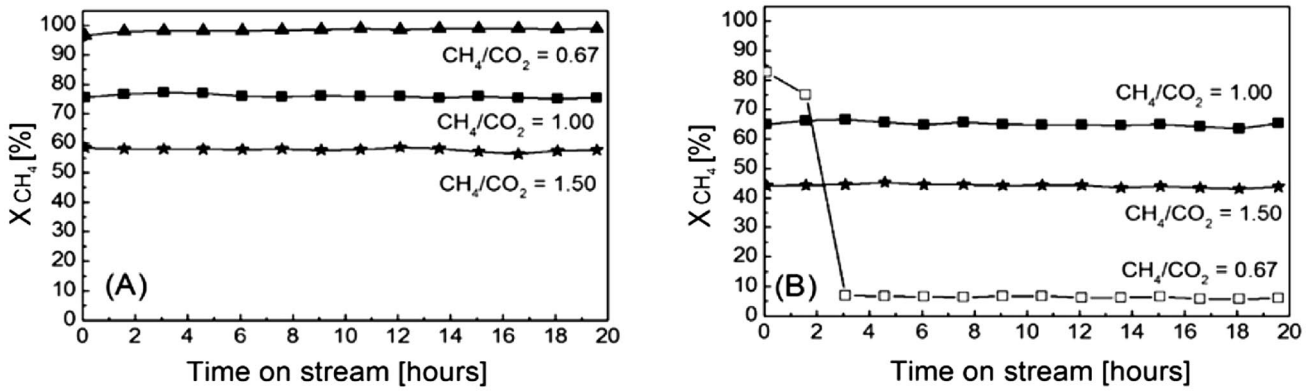

Dry Reforming of Methane over Ni-WC (A) and Ni-Mo_2C (B) catalysts

Effects of Variation in CH_4/CO_2 Molar Ratio (P = 1 atm and T = 800 ºC)

Keywords Ni–carbide · Carbon dioxide reforming · DRM · Hydrotalcite–like precursor

1 Introduction

Natural gas (NG) consists mainly of methane (70–98% CH_4) and other hydrocarbons (C_2–C_4) and stands out among the fossil sources of energy due to its abundance [1–5]. It is worth mentioning that, in some regions, extracted NG could contain contaminants, such as CO_2 and H_2S. For example, Brazil's reserves located in ultra–deep waters (pre–salt layer) have typically high concentrations CO_2, up to 45% [6–8],

Victor Luis dos Santos Teixeira da Silva in memoriam

✉ Fabio Barboza Passos
fabiopassos@id.uff.br

[1] Núcleo de Catálise, Programa de Pós–Graduação em Engenharia Química (NUCAT/PEQ/COPPE), Universidade Federal Do Rio de Janeiro (UFRJ), RJ, Brasil

[2] Laboratório de Reatores, Cinética e Catálise, Departamento de Engenharia Química e de Petróleo (RECAT / TEQ), Universidade Federal Fluminense (UFF), Niterói, Brasil

or, in the case of Natuna D–Alpha Indonesia gas field, CO_2 concentration may reach 71% [9].

Besides, when NG is associated with oil or in remote locations, the costs of purification, compression, storage, and transportation can make its exploration economically unattractive [3, 6]. For these reasons, NG is sometimes reinjected into the wells, stimulating the recovery of oil or even flared without use [6]. The volume flared of NG was estimated, in 2017, to be 140.6 billion m^3 [4]. Although this volume is decreasing around the world, it represents, for example, 3.7 times the Brazilian consumption of NG in the same year (38.3 billion m^3) [4].

The conversion of methane into value-added chemicals has been a matter of great interest to the industry and academy [2, 3, 10]. However, it often becomes desirable to transform NG into liquid products at the production site, in order to facilitate transport and storage. In this context, steam reforming of methane (SRM, $CH_4 + H_2O$ $3H_2 + CO$), dry reforming of methane (DRM, $CH_4 + CO_2$ $2H_2 + 2CO$) and partial oxidation of methane (POM, $CH_4 + 1/2O_2$ $2H_2 + CO$) are all suitable methods for the production of synthesis gas ($H_2 + CO$). Syngas, also produced by gasification and pyrolysis of carbonaceous materials (coal and biomass), is the most significant intermediate for the production of hydrogen, ammonia, and methanol, as well as of liquid hydrocarbons by Fischer–Tropsch synthesis [3, 5, 8, 11–18]. SRM process has been the preferred commercial technology for this purpose over decades [3, 11, 16]. However, combinations of the mentioned processes, such as the autothermal reforming of methane (SRM + POM or DRM + POM) [19] and the combined methane reforming (DRM + SRM + POM) [20] were also developed to increase energy efficiency. Additionally, reverse water–gas shift (RWGS, $CO_2 + H_2$ $CO + H_2O$), Boudouard reaction (BR, $2CO$ $C + CO_2$) and methane decomposition (MD, CH_4 $C + 2H_2$) are side reactions that can influence the composition of products in methane reforming, depending on catalytic system and reaction conditions used [21].

Although DRM produces syngas with low H_2/CO ratio ($H_2/CO \cong 1$), when compared to SRM ($H_2/CO \cong 3$) and POM ($H_2/CO \cong 2$), it is a suitable ratio for direct use in processes such as synthesis of hydrocarbons by Fischer–Tropsch reaction, synthesis of methanol, ammonia [10, 13] and dimethyl ether. The latter is a promising alternative to replacement diesel [16]. Among DRM advantages over SRM and POM is the possibility of using NG, or biogas, without additional processing to remove CO_2 [8, 10, 13, 17]. Biogas (or landfill gas) is another important source of methane associated with carbon dioxide, generated by anaerobic decomposition of organic matter in the presence of methanogenic bacteria, and is composed mainly of CH_4 (40–70%) and CO_2 (30–60%) [10, 16]. DRM also allows the use of the recycle stream of Fischer–Tropsch processes, which may contain CH_4 and CO_2 [5]. Finally, the operational costs of this process are estimated to be reduced by up to 20% compared to the other reforming processes [17]. Thus, the DRM process presents a potential for industrial application and is attractive for the conversion of the two gases with high impact in the greenhouse effect, CH_4 and CO_2, into syngas [11, 13, 15–17].

Despite many advantages in DRM, its potential for carbon formation over catalysts is much higher than in SRM [22], and its industrial application on a large-scale is still limited to a few process such as CALCOR and SPARG [14, 23]. Both process are conducted into catalyst fired–tubes (similar to a standard SRM device), at high temperatures (up to 1000 ºC) and pressures in the range of 1–20 bar [22]. CALCOR process, from Caloric Anlagenbau GmbH, can be operated under low pressure to produce syngas with low H_2/CO ratio (as low as 0.4 to obtain pure CO), using, for example, CO_2 recovered from reformer flue gas by an amine acid gas removal system [24]. SPARG process (**S**ulfur **PA**ssivated **R**eformin**G**), from Haldor–Topsoe, produce syngas with H_2/CO ratio from 0.6 to 1.0, and, the carbon deposition over Ni catalyst is minimized by partially poisoning them with sulfur, by H_2S addition to the feed (CH_4/CO_2) [25]. Often, DRM is combined with SRM, avoiding carbon deposition and allowing to control syngas composition with H_2/CO ratios of 2 or lower [25, 26].

Great efforts have been moved during the last few decades to develop suitable DRM catalysts, with high activity, low cost, and stability for long periods [27]. Traditional catalysts used in industrial methane reforming, in general, are composed of nickel supported on alumina or calcium/magnesium aluminates. Despite having high catalytic activity (fast turnover rates), these catalysts tend to deactivate by sintering at high operating temperatures and, mainly, by carbon deposition. This loss in catalyst activity is due to both the blocking of active nickel sites and the catalytic bed clogging [1, 2, 10, 11, 13, 17, 18]. According to the literature [1, 28], there is a trend to use an excess of oxidant in the reaction feed to minimize deactivation, promoting carbon gasification. Other strategies to overcome the problem of carbon deposition propose the combination of different supports (CeO_2, ZrO_2, MgO, $MgAl_2O_4$), the addition of small amounts of promoters (noble metals and alkaline metals) or partial passivation with sulfur [1, 10, 11, 13, 18, 28]. Noble metals (Ru, Rh, Ir, Pd, and Pt) supported catalysts have high activities (fast turnover rates) in DRM and, although more resistant to carbon deposition, they are economically impracticable for large–scale application [1, 8, 10, 13, 16, 29].

Finally, another point to be emphasized is traditional catalysts are not stable when the CH_4/CO_2 molar ratio greater than 1. In general, CH_4 and CO_2 are not in the equimolar ratio in sources such as biogas and NG, so a catalysts active and stable under an excess of CH_4 or CO_2 would be attractive to industrial apply [30]. Besides, both nickel and noble

metal catalysts are also irreversibly deactivated in the presence of sulfur compounds [31, 32], frequently found as H_2S in both NG and biogas [8, 33]. On the other hand, transition metal carbides, whose precursors are relatively inexpensive and abundant [5, 11], present catalytic activities comparable to noble metals in DRM [1, 3], as well as being resistant to sulfur poisoning [32, 34]. Recent theoretical and experimental studies have shown beneficial interactions of a transition metal with a transition metal carbide, that result in beneficial effects such as: promotion of CO_2 reduction, by reducing C-O bond scission barrier, over monolayer Cu promoted WC [35]; and promotion of CH_4 activation, by reducing C-H bond scission barrier, even at room temperature, over layered TiC promoted by Ni clusters [36].

According to the literature [1, 3], molybdenum and tungsten carbides are stable with high catalytic activity ($Ru > Rh > \beta–Mo_2C \cong Ir > \alpha–WC > Pd > Pt$) when applied to DRM ($CH_4/CO_2 = 1$) at elevated pressures (P = 8 atm). However, they may suffer rapid deactivation due to carbide oxidation by CO_2 at atmospheric pressure [1–3]. In fact, at DRM standard operation temperature range, carbides could be obtained by exposing oxides to CH_4, and oxides could be obtained by exposing carbides to CO_2, indicating that metal carbides could function as redox catalysts for DRM [3, 15]. The addition of Ni or Co to these Mo and W carbides can be a way to increase the activity and stability in DRM at atmospheric pressure [5, 12, 13, 15, 17, 18].

Despite presenting carbon deposition [5, 17], the mixed carbide Co_6W_6C becomes active after segregation of Co and WC phases. Although Co–W-C and Ni–W-C catalysts present a tendency to graphitic carbon formation over the surface during DRM, this carbon does not deactivate the catalysts, and it could also be pointed as reason of its final activity and stability [12]. On the other hand, when molybdenum carbide was promoted by nickel or cobalt, in a specific proportion ($Ni_{0.2}Mo_{0.8}C_x$ or $Co_{0.4}Mo_{0.6}C_x$), it became an active and stable system in DRM at atmospheric pressure, without carbon deposition [13]. However, when a similar Ni–Mo_2C ($Ni_{0.2}Mo_{0.8}C_x$) was employed in DRM with a non–stoichiometric feed (CH_4/CO_2 molar ratio of 0.67 or 1.5), there was deactivation by Mo_2C oxidation to MoO_2 and MoO_3 [18].A series of catalysts composed of Ni–Mo_2C and Ni–WC (Ni/M = 1/2, 1/9 and 1/21, where M are Mo or W) were evaluated in DRM and results shown them as active and stable, with exception of Ni/Mo = 1/21 that deactivated by oxidation of Mo_2C. Ni-WC showed better control of crystal structure, resisting to sintering (hypothesized as the reason of deactivation), when compared to Ni-Mo_2C (despite Mo_2C oxidation) [15].

No previous studies were found applying Ni–WC in DRM, under high or atmospheric pressure, employing a non–equimolar reactional feed ($CH_4/CO_2 \neq 1$). The ability to operate with different feed compositions is primordial, because, besides the fact that carbon dioxide composition varies in natural sources of methane, in industrial applications the reactant composition may vary along the catalytic bed.

In this context, we report here the effects of variation of the CH_4/CO_2 molar ratio, from 0.67 to 1.5, on the catalytic performance of nickel promoted molybdenum or tungsten carbides (Ni–Mo_2C and Ni–WC) in dry reforming of methane (DRM) at atmospheric pressure.

2 Experimental Methodology

2.1 Catalyst Precursor Preparation

NiMo and NiW catalysts precursors were obtained by co-precipitation from aqueous solutions of nickel nitrate [$Ni(NO_3)_2.6H_2O$] and ammonium heptamolybdate [$(NH_4)_6(Mo_7O_{24})0.4H_2O$] or ammonium paratungstate [$(NH_4)_{10}(H_2W_{12}O_{42})0.4H_2O$], in amounts such as to obtain unitary metal molar ratio (Ni/Mo = 1 or Ni/W = 1). The initial pH of these solutions was adjusted (pH = 10) by the addition of ammonium hydroxide (NH_4OH), resulting in a solution of intense blue color. This solution was heated up to 100 °C under magnetic stirring and boiled under reflux (20 ºC). Over time, a green precipitate was formed. When the pH of the suspension reached values close to 7, about 4 h later, the heater was switched off. Then, the system was kept under stirring for 15 h at room temperature (25 °C). The resulting precipitate, after filtration under vacuum, was dried at 120 ºC for 24 h. Finally, a pale green fine powder was obtained after calcination under N_2 atmosphere at 300 ºC for 1 h.

2.2 Catalysts Activation–Synthesis of Carbides

The carbides were obtained from NiMo and NiW catalysts precursors using temperature programmed carburization (TPC) technique, under a flow of carburization mixture (150 mL min^{-1}, 20% v/v CH_4/H_2, W/F = 0.0556 g h L^{-1}). The samples (0.5 g) of catalysts precursors, conditioned in a "U" shaped quartz reactors (1 cm diameter), were heated at a rate of 2.5 ºC min^{-1}, from room temperature (25 ºC) to the final temperature (650, 750 and 850 ºC), remaining isothermally for 2 h at this temperature. Due to the pyrophoric character of the carbides, the samples were passivated for 15 h under a 10 mL min^{-1} flow of 0.5% O_2/N_2 just after the synthesis to allow the characterization in atmospheric conditions.

2.3 Catalytic Activity Tests

The experimental unit was composed of a gas controller system, connected in series to a U-shaped quartz reactor (1 cm diameter) and a gas chromatograph (GC). A Bronkhorst mass flow regulator model E-75000-RDD controlled the flow of reactant (CH_4, CO_2) and of internal standard (N_2). The quartz reactor inside a tubular electric oven operated at atmospheric pressure and controlled temperature (THERMA TH 90DP-201-000 controller).

An inline gas chromatograph (Shimadzu, GC-2014) equipped with a thermal conductivity detector (TCD) was used to determine the composition of products and reactants (in dry base) employing two systems for separation: (1) a Supelco capillary separation column, Carboxen–1010 plot (30 m × 0.32 mm # 35,789–02A), having H_2 as a carrier gas; (2) a Varian molecular sieve capillary column, CP–Molsieve 5A (25 m × 0.53 mm # CP7538), using argon as a carrier gas. Before the GC inlet, the gas flow was dried using a cold trap.

Before catalytic evaluation, the samples were carburized in–situ at 850 °C (as described in Sect. 2.2) and cooled to 800 ºC under a N_2 flow of 50 mL min^{-1}. Reaction feeds with different CH_4 and CO_2 concentrations [% v/v] were used according to Table 1, keeping 20% of N_2 as the internal standard, in a total flow of 50 mL min^{-1}. The effluent from the reactor, dried in a cold trap, was periodically analyzed: the first GC analysis was carried out 5 min after starting the reaction and regularly at every 1.5 h on stream, until 20 h.

The catalytic performance was evaluated in terms of reactant conversion (X %), products selectivity ratio (H_2/CO ratio) and H_2 yield (%), at the outlet of the reactor, as following equations.

$$X_{CH_4}\ \% = \frac{\eta_{CH_{4_{inlet}}} - \eta_{CH_{4_{outlet}}}}{\eta_{CH_{4_{inlet}}}} \times 100 \quad (1)$$

$$X_{CO_2}\ \% = \frac{\eta_{CO_{2_{inlet}}} - \eta_{CO_{2_{outlet}}}}{\eta_{CO_{2_{inlet}}}} \times 100 \quad (2)$$

$$H_2/_{CO}\ Ratio = \frac{\eta_{H_{2_{outlet}}}}{\eta_{CO_{outlet}}} \quad (3)$$

Table 1 Feed composition used in catalytic runs [% v/v]

Test	[CH_4]	[CO_2]	[N_2]	CH_4/CO_2
1	48	32	20	1.50
2	40	40	20	1.00
3	32	48	20	0.67

$$H_2\text{Yield}\ \% = \frac{\eta_{H_{2_{outlet}}}}{2.\left(\frac{\eta_{CH_{4_{inlet}}} - \eta_{CH_{4_{outlet}}}}{\eta_{CH_{4_{inlet}}}}\right)} \times 100 \quad (4)$$

2.4 Characterization

The catalyst precursors and the carbide activated catalysts were characterized by different techniques, before and after the catalytic runs (fresh and expended catalysts).

2.4.1 X-ray Fluorescence (XRF)

The metal contents of the catalyst precursors (Ni, Mo or W) were determined using a Rigaku X-Ray fluorescence spectrometer, model RIX3100, operating with a rhodium anode X-ray tube, 4 kW (150 mA).

2.4.2 X-ray Diffraction (XRD)

XRD analysis were performed in a Rigaku X-ray diffractometer, model Miniflex, using CuKα X-ray radiation (λ = 1,54 Å), varying the diffraction angle (2θ) continuously, at a speed of 2° min^{-1}, a step of 0.05º, in the 10º < 2θ < 90º range. Phase identification was performed using the Jade-5 software, by comparing the X-ray diffraction patterns with standard crystallographic datasheets from ICDD (The International Center for Diffraction Data).

2.4.3 Nitrogen Physisorption

Specific surface area (S_g), pore volume and diameter (V_p, D_p), were estimated from nitrogen isotherms obtained using BET and BJH methods, respectively, in a Micromeritcs ASAP 2020 device. Before analysis, the samples were pre–treated (dried) under vacuum at 110 °C.

2.4.4 Fourier Transform Infrared Spectrometry (FTIR)

FTIR analyses were carried out in a Perkin Elmer Spectrum–100 spectrometer, operated in the medium infrared region (4000–400 cm^{-1}), using a DTGS detector. A total of 32 scans were performed in each sample, with a resolution of 4 cm^{-1}.

2.4.5 Raman Spectroscopy (Raman)

The nature of carbon species present in activated carbide samples, before and after the catalytic evaluation, was identified employing a Horiba Jobin Yvon Raman spectrometer (HR800UV) equipped with a red laser He–Ne (632 nm), CCD detector (cooled to − 70 °C). An Olympus BX41

optical microscope was responsible for the laser focus over the samples, performed using a magnification lens of 100 times with optical density filter D1. The spectroscopic data were detected on a region of 1000–1800 cm^{-1}, with a slit of 100 µm and recorded with a 50 s exposure time over 32 scans.

2.4.6 Temperature Programmed Studies (TPS)

TPS experiments were carried out in a multipurpose unit, including a gas control system, a quartz reactor and a quadrupole mass spectrometer (MS). The feed was set up by 4-channel mass flow meter, MKS-247, allowing the use of pure gases or mixtures. A U-shaped quartz reactor (1 cm diameter) operated at atmospheric pressure inside in a tubular oven with controlled temperature (THERMA TH90DP–201–000 controller). Before the experiments, the samples were dried in–situ under the flow of 50 mL min^{-1} at 110 °C for 1 h with a heating rate of 10 °C min^{-1}. The reactor effluent was continuously analyzed by a Pfeiffer Vacuum, QME 200 mass spectrometer. The ion signals (m/z) representative of various molecular species monitored were: H_2: 2 (100%); He: 4(100%); CH_4: 16 (100%); 15 (85.8%); NH_3: 17 (100%), 16 (80%); H_2O: 18 (100%); 17 (23%); N_2: 28 (100%); and, CO: 28 (100%).

2.4.6.1 Temperature Programmed Decomposition (TPDec) Thermal decomposition of the catalysts precursors was studied by analyzing the desorbed gases during calcination. Samples (500 mg) of fresh (uncalcined) catalysts precursors were heated from room temperature (25 °C) up to 300 °C under the flow of 75 mL.min^{-1}, remaining isothermally for 1 h at the final temperature.

2.4.6.2 Temperature Programmed Carburization (TPC) TPC was employed to study the carburizing phenomena and temperatures of the catalyst precursors (calcined at 300 °C) in a flow of 20% CH_4/H_2 (**TPC with CH_4/H_2**) or a flow of 50% CH_4/He (**TPC with CH_4/He**). In both cases, 100 mg samples were heated from 25 ºC to 900 °C at a rate of 2.5 °C min^{-1} under a flow of 100 ml min^{-1} of the chosen gas mixture.

2.4.6.3 Temperature Programmed Oxidation (TPO) TPO with CO_2 was used to study the profile of carbides oxidation. Under 100 ml min^{-1} flow of 50% CO_2/He, 100 mg carbide samples (carburized at 850 °C and passivated) were heated (rate of 2.5 °C min^{-1}), from 25 ºC to 900 °C.

2.4.7 Chemisorption of CO

After the activation at 850 °C (under previously described conditions), the carbide sample was cooled to room temperature under a 50 mL min^{-1} flow rate of He, and then subjected to pulses of 2.39 mL of 5% CO/He mixture until surface saturation.

3 Results and Discussion

3.1 Characterization of Catalyst Precursor

According to XRF results, the NiMo catalyst precursor (dried at 120 °C) was composed of 55.1 wt% NiO and 44.8 wt% MoO_3, corresponding to a Ni:Mo molar ratio of 2.4; NiW (dried at 120 °C) presented a composition of 36.6 wt% NiO and 63.4 wt% WO_3, corresponding to a Ni:W molar ratio equal to 1.8. These ratio values are much higher than the desired (Ni:Mo = Ni:W = 1), indicating that part of the molybdenum (or tungsten) was not incorporated into the formed solid during the precipitation stage, remaining in solution.

XRD results of catalyst precursors (Fig. 1) did not show characteristic diffraction of segregated oxides (NiO, MoO_3 or WO_3) with long range order crystalline structures. NiW diffractogram (dried at 120 °C, Fig. 1b) showed low–intensity peaks, attributed to thermally unstable phases (such as ammonium nickel tungsten hydrogen oxide hydrate), that were decomposed after calcination at 300 °C (Fig. 1a) resulting in a low crystallinity structure. NiMo diffractogram (dried at 120 °C, Fig. 1d), on the other hand, exhibited the presence of a better–organized structure that could be attributed to a turbostratic layered nickel hydroxide α–$Ni(OH)_2xH_2O$, with broad and low intense diffraction peaks, at 34.5 and 60.5º, related to the planes (111) and (301), respectively [37]. In this case, the calcination step at 300 °C did not result in visible changes in the diffractogram (Fig. 1c).

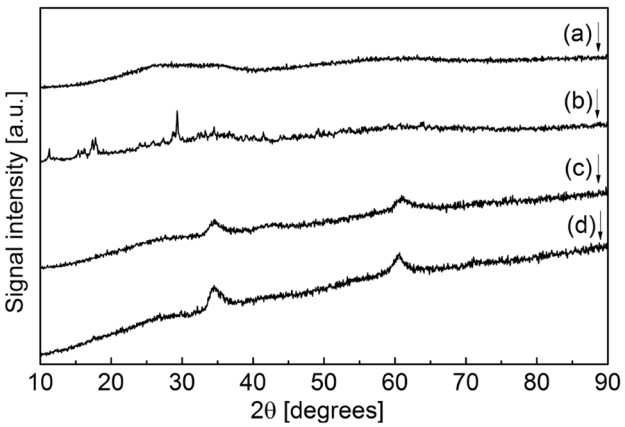

Fig. 1 XRD of catalysts precursors: (**a**) NiW calcined at 300 °C; (**b**) NiW dried at 120 °C; (**c**) NiMo calcined at 300 °C; (**d**) NiMo dried at 120 °C

The obtained N_2 isotherms for the NiMo catalyst precursor (not shown), before and after calcination, can be classified as type IV (second IUPAC classification), characteristic of mesoporous materials ($20 < D_P < 500$ Å) with strong adsorbent/adsorbate interaction. These isotherms showed hysteresis type H3, characteristic of materials formed by aggregated particles in the form of plates, with narrow pores of the slit type [38]. The calcination of the NiMo sample at 300 °C increased BET specific area (S_g), from 11 to 22 $m^2\ g^{-1}$, and BJH pore volume (V_p), from 0.04 to 0.05 $cm^3\ g^{-1}$. The isotherms obtained for NiW catalyst precursor (dried and calcined) were classified as type III, characteristic of nonporous or macroporous materials ($D_P > 500$ Å), with low adsorbent/adsorbate interaction [38]. In the case of NiW sample, the calcination at 300 °C did not cause significant changes in specific area, which can be considered negligible in both cases ($S_g < 10\ m^2\ g^{-1}$).

FTIR analysis of NiMo and NiW catalysts precursors (Fig. 2) showed vibrational modes associated with H_2O, OH^-, NO_3^- and NH_4^+ groups. The wavenumber region between 3700–2700 cm^{-1} encompasses vibrations associated with axial deformation (stretching) of hydrogen bonded to oxygen (O–H) and nitrogen (N–H) atoms. The weak and wide bands in this region may be related to: harmonic vibrations or overtones, with wavenumbers two times higher than that of strong bands in the region between 1800–1300 cm^{-1}; weak hydrogen bonds (near 3440–3460 cm^{-1}) [39]; and stretching of OH groups without hydrogen bonding (3650 cm^{-1}) [40]. Vibrations in the region between 3300–3050 cm^{-1} may be related to the asymmetric N–H stretching [41].

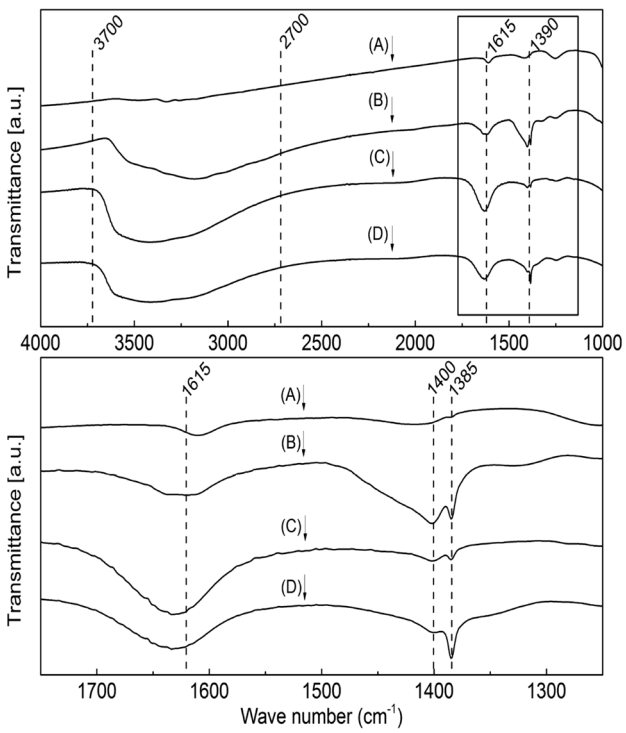

Fig. 2 FTIR–of catalysts precursors: (**a**) NiW calcined at 300 °C; (**b**) NiW dried at 120 °C; (**c**) NiMo calcined at 300 °C; (**d**) NiMo dried at 120 °C

The FTIR band near 1615 cm^{-1}, more pronounced in the NiMo sample, corresponds to the symmetrical angular deformation in the plane of H_2O molecules [40]. The presence of ammonium ions (NH_4^+) was more pronounced in the NiW sample, as evidenced by the observations of asymmetric N–H stretching in the region between 3300 and 3050 cm^{-1} and angular deformation H–N–H near 1400 cm^{-1} [41]. The presence of nitrate ions (NO_3^-) can be identified by a pronounced peak, related to asymmetric stretch N–O, near 1385 cm^{-1} [39], more evident in the case of NiMo sample.

The results obtained by FTIR after the calcination at 300ºC indicated a strong reduction in the vibration intensities related to hydroxyl (OH^-), ammonium (NH_4^+), nitrate (NO_3^-) and H_2O species initially present in the samples.

TPDec profiles (Fig. 3), simulating the calcination process at 300 °C, showed releases of H_2O (w/z = 18 and 17), NH_3 (w/z = 17 and 16) and N_2 (m/z 28). The profile obtained for the NiMo catalyst precursor showed a more intense formation of w/z = 28, which may be associated to N_2 species originated from the decomposition of NO_3^-. The NiW profile, in turn, showed a more intense release of w/z = 17 and 16, which may be related to NH_3 formation. Both profiles displayed intense H_2O release (w/z = 18 and 17). TPDec results (Fig. 3) corroborate those of FTIR (Fig. 2), showing that the NiMo and NiW samples differed in relation to the amount of H_2O and NH_4^+ and NO_3^-.

Nickel hydroxides may exhibits polymorphism in varied crystallographic structures [37, 40]. The so-called nickel(II) beta–hydroxide [β–$Ni(OH)_2$], consists of parallel layer of $Ni(OH)_2$ separated by interlamellar ions, which remain bound to the hydroxides by hydrogen bonds. Other nickel(II) hydroxides, such as alpha–hydroxide [α–$Ni(OH)_2$], present excess interlamellar ions and result in less crystalline materials. This lower crystallinity observed in some hydroxides can be attributed to the formation of a turbostratic structure, in which the basal planes are randomly displaced between each other, increasing the spacing between these planes. In such hydroxides, the presence of water molecules is essential for the structural formation, positioned in an intercalated manner with OH^- groups of the $Ni(OH)_2$ hydroxide layer, remaining bonded to these OH^- groups by hydrogen bonds [40].

There are reports in the literature about the occupation of the interlamellar spaces of lamellar double hydroxides, being observed the occurrence of molybdenum oxometalates (MoO_4^{2-} at pH > 7) and tungsten oxometalates (WO_4^{2-} at pH > 8, $W_{12}O_{42}^{12-}$ at pH 7,8, $W_{12}O_{29}^{6-}$ at pH 5,7) [42].

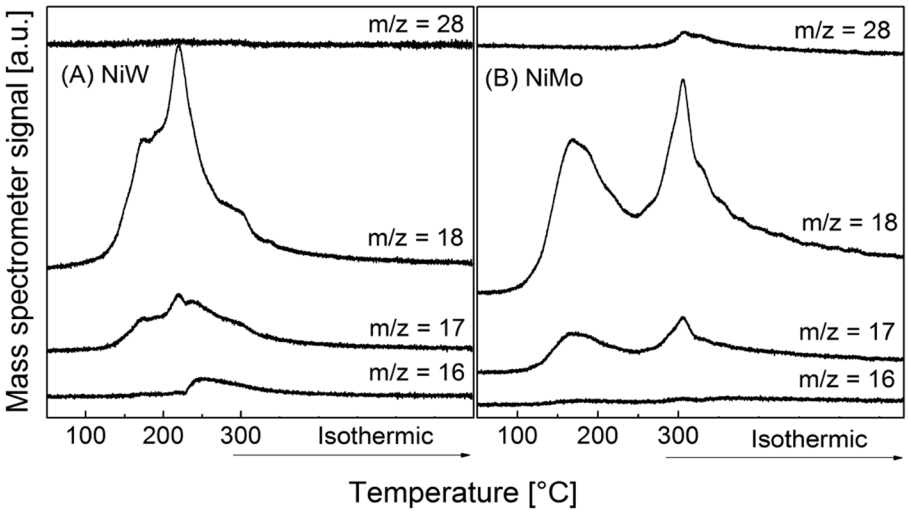

Fig. 3 TPDec– (**a**) NiW and (**b**) NiMo (catalyst precursors dried at 120 °C)

The random displacement of the basal planes in turbostratic hydroxide can generate anionic and/or cationic vacancies in the galleries between the lamellae that can be compensated by a variety of ions (H_2O, NH^{4+}, NO^{3-}, OH^-, MoO_4^{2-}, WO_4^{2-}, $W_{12}O_{42}^{12-}$and $W_{12}O_{29}^{6-}$) present in the mother liquor. Based on the characterization results (XRF, XRD, and FTIR), together with literature results [40–42], it was assumed that the catalysts precursors NiMo and NiW were composed of nickel hydroxide and ammonium molybdate (or tungstate). These precursors possibly presented a nickel turbostratic–structured oxy–hydroxide [α–Ni $(OH)_2$] intercalated by oxometalates of molybdenum or tungsten.

TPC profiles (Fig. 4) indicated changes in the reduction/carburization temperatures of NiMo and NiW catalysts precursors as compared to isolated oxides (NiO, MoO_3, and WO_3). According to the literature the carburization process of MoO_3 and WO_3 oxides occurs in two steps, being initiated by the reduction of MeO_3 to MeO_2 (where Me = Mo or W) with H_2O release; then, in a second step, the reduction/carburization of MeO_2 to Me_xC_y occurs, with CH_4 consumption [34].

During the carburization of NiMo and NiW catalysts precursors, the reduction process of Mo and W oxides was facilitated by the contact with Ni, which in turn had its reduction affected, when compared to the pure oxides. The observed release of w/z = 28 can be attributed to the production of CO, which proves the consumption of CH_4 in two regions, unlike that observed for pure oxides (MoO_3 and WO_3). The known carbon deposition process on metallic nickel may have facilitated the reduction of Mo and W oxides during TPC, which is in accordance with previously reported results in the literature [43]. Such changes in the temperatures of carburization and reduction could be attributed to the intimate contact of the oxides generated by the good dispersion of the cations and to the existence of strong metal–metal interaction in NiMo and NiW samples.

3.2 Characterization of the Fresh Catalysts

XRD analysis reveals the structures of NiW and NiMo catalysts become more crystalline after activation (Fig. 5), resulting in a combination of heterogeneous phases. When NiW carburized at 650 °C, there was the formation of Ni^0 (PDF # 04-0850) and β–W_2C (PDF # 35-0776) phases. When the carburizing temperature increased to 750° C and 850 °C, there was a tendency towards formation of α–WC (PDF # 25-1047), β–W_2C and Ni^0, besides pyrolytic carbon as graphite (PDF # 41-1487).

NiMo, on the other hand, formed Ni^0 and β–Mo_2C phases (PDF # 35-0787) at any tested carburizing temperatures (650, 750 and 850 °C). Thus, the higher the final carburization temperature, the diffraction peaks become sharper (smaller FWHM—Full Width at Half Maximum) and increased the intensities, indicating crystallite grow. These characterize a sintering process. As reported in the literature [2], the α–WC/β–W_2C and β–Mo_2C phases occurred from TPC of CH_4/H_2 on tungsten and molybdenum oxides. Besides, Ni–W–C or Ni–Mo–C solid solutions may also have been formed [34]. Thus, for the catalytic evaluation, the carburization was conducted at 850 ºC to minimize structural alterations by sintering.

The results of N_2 adsorption for the carbides samples (passivated after carburization at 850 ºC) indicate that Ni–Mo_2C presented low BET specific area ($S_g < 10\ m^2\ g^{-1}$) and its isotherm (not shown) can be classified as type III, are characteristic of nonporous or macroporous materials. Ni–WC samples exhibited a specific surface area of 25 $m^2\ g^{-1}$ and BJH pore volume of 0.09 $cm^3\ g^{-1}$ with isotherm type IV and H3 hysteresis, characteristic of micro and mesoporous materials (similar as discussed above).

NiMo and NiW samples freshly carburized at 850° C (not passivated) presented negligible values of CO chemisorption, which can be attributed to the presence of pyrolytic/

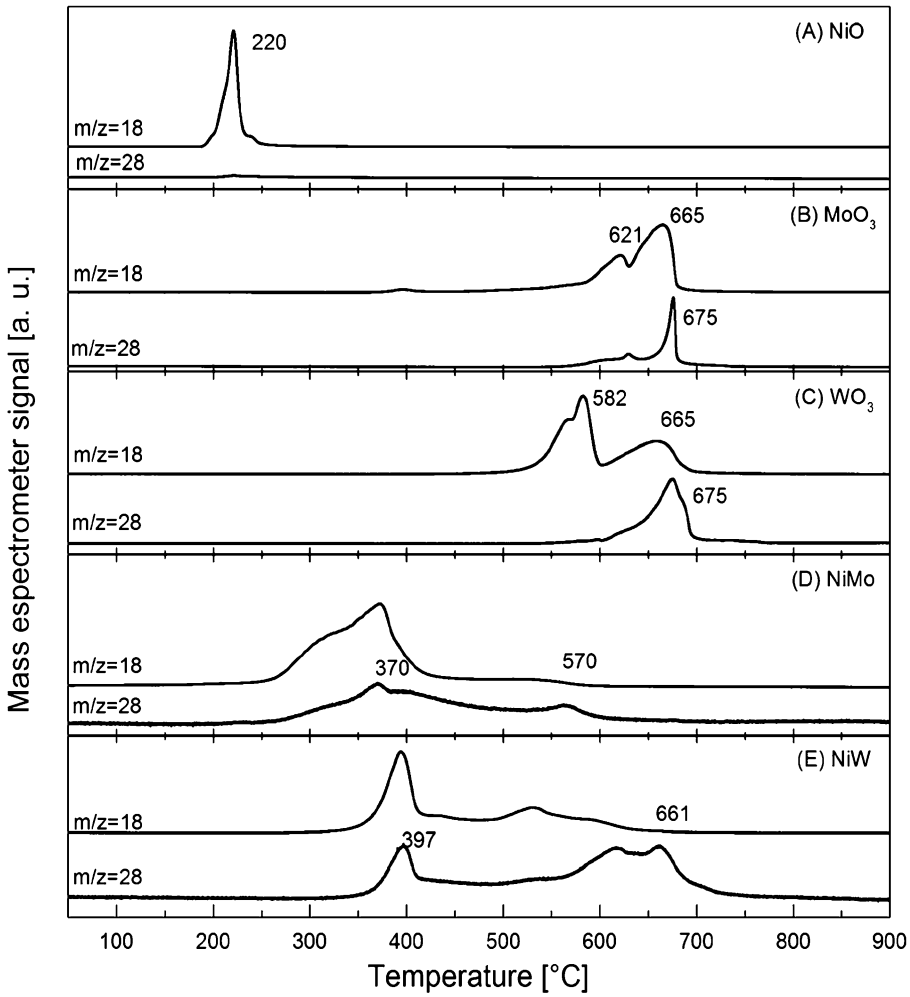

Fig. 4 TPC (20% CH_4/H_2) profiles for isolated oxides: (**a**) NiO; (**b**) MoO_3; (**c**) WO_3; and catalysts precursors (**d**) NiMo; (**e**) NiW

polymeric carbon coating the surface of the samples, as previously reported in the literature [44].

3.3 Expended Catalysts Characterization

Post–reaction XRD analysis of Ni–WC (Fig. 6), in the case of equimolar proportions of the reactant ($CH_4/CO_2 = 1$) or excess of CH_4 ($CH_4/CO_2 = 1.5$), revealed the presence of metallic nickel (Ni^0), carbides (α–WC and β–W_2C), and graphite carbon. However, when an excess of CO_2 ($CH_4/CO_2 = 0.67$) was employed, while Ni^0 and α–WC phases remained the same, there was a decrease in peak diffraction intensity of the β–W_2C and pyrolytic carbon (graphite) phases.

XRD patterns of Ni–Mo_2C after reaction (Fig. 6) displayed metallic nickel (Ni^0) and molybdenum carbide (β–Mo_2C) for feed reactants mixtures with stoichiometric ratio ($CH_4/CO_2 = 1.0$) or excess of CH_4 ($CH_4/CO_2 = 1.5$). For excess of CO_2 ($CH_4/CO_2 = 0.67$), there was the presence of MoO_2, due to the oxidation of β–Mo_2C, while Ni^0 phase was not affected. Besides, no pyrolytic carbon (graphite) was detected by XRD of Ni–Mo_2C after reaction, for all reactants mixtures used as feed.

Figure 7 presents the Raman spectra for Ni–WC and Ni–Mo_2C samples before (fresh) and post–reaction (expended). Resonance G (≅1580 cm^{-1}), D (≅1330 cm^{-1}) and D' (≅1620 cm^{-1}) bands, characteristic of the presence of non–diamond carbon (graphite or amorphous), are identified in the spectra. The ratio between the intensities of D and G bands (I_D / I_G) is used as an indicator of the degree of structural disorder. Broad D and G bands are characteristic of graphitic carbon, the wider these bands in the spectrum, the more amorphous the material [45]. The I_D / I_G ratio increase for both catalysts Ni–WC and Ni–Mo_2C after the reaction runs. This increase may be related to a larger organization of the pyrolytic carbon structures present as graphite or amorphous form. However, the catalytic performance was not strongly dependent on these results. This region of Raman spectra (1200 to 1800 cm^{-1}) was not adequate to evaluate carbidic carbon formation.

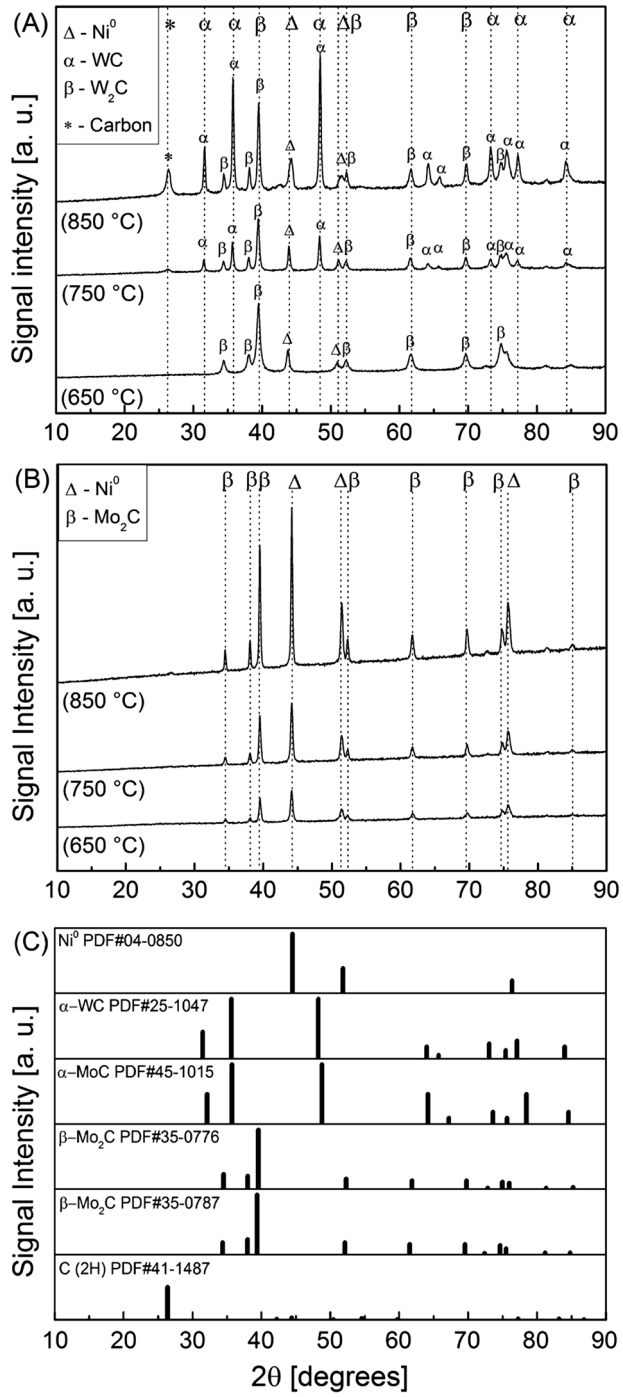

Fig. 5 XRD patterns– (**a**) NiW, (**b**) NiMo–carburized at 650, 750 and 850 °C, and (**c**) standard reference lines

Raman results (Fig. 7) corroborate with those observed by XRD (Fig. 6), confirming significant carbon formation on Ni–WC after reaction with CH_4 /$CO_2 \geq 1$ and, also, the removal of carbon from Ni–Mo_2C when used in excess of CO_2, culminating with carbide oxidation.

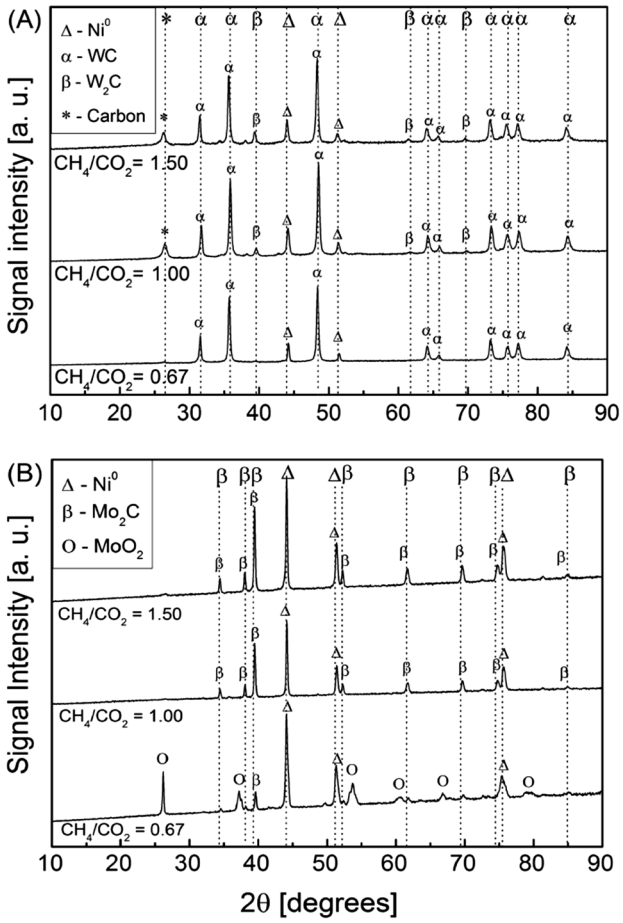

Fig. 6 Post-reaction XRD patterns of Ni–WC (**a**) e Ni–Mo_2C (**b**) – expended samples

3.4 Complementary Characterization

TPR with CH_4/He (Fig. 8) results revealed NiMo catalyst precursor exhibit the formation of H_2O (w/z = 18) and CO (w/z = 28), indicative of reduction/carburation, at temperatures lower than NiW catalyst precursor. The XRD analysis performed on these samples after TPC with CH_4/He (results not presented) revealed they were effectively carburized.

CO_2/He–TPO results (Fig. 9) for Ni–Mo_2C and Ni–WC carburized at 850 ºC showed the release of CO as indicative of carbon oxidation. Ni–Mo_2C was oxidized at a temperature slightly lower than Ni–WC (617 ºC and 673 ºC, respectively). However, the results did not possible allow to distinguish the oxidation peak of the different carbon species present (pyrolytic and carbidic), as Shi et al. (2012) have described in the literature [46]. The oxidation temperatures observed in the present work are slightly lower than those registered by Shi et al. (2012) for pyrolytic carbon (675–689 °C) and carbidic carbon (856–854 °C) [46]. Such differences can be attributed to the different values

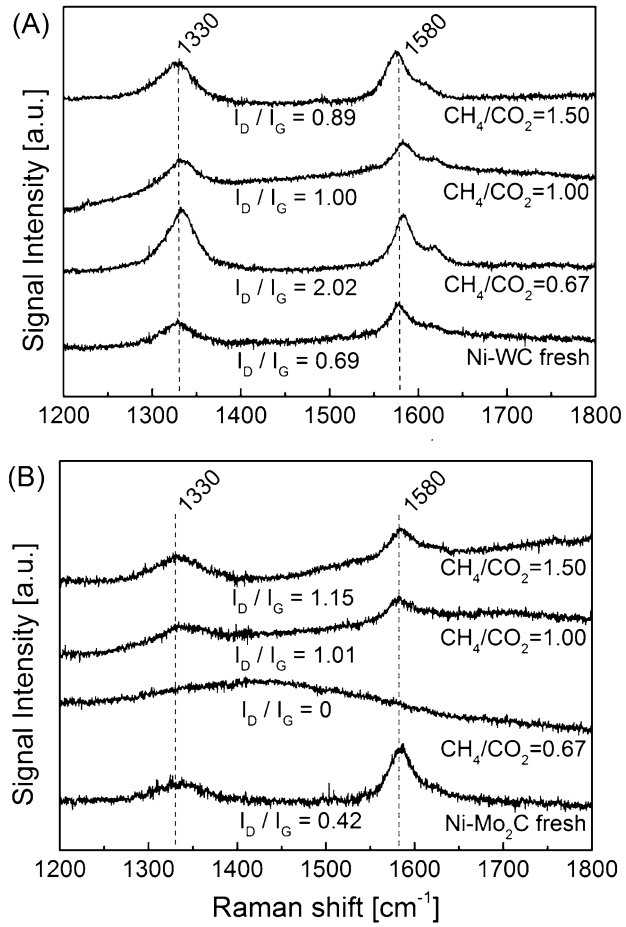

Fig. 7 Raman spectra of Ni–WC (**a**) and Ni–Mo_2C (**b**) before and post-reaction

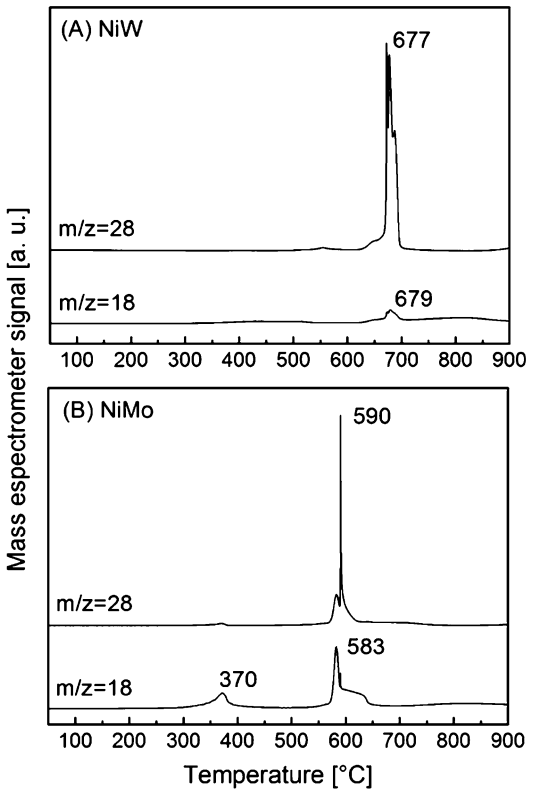

Fig. 8 CH_4/He–TPC profiles: (**a**) NiW and (**b**) NiMo (calcined at 300 ºC, oxide form)

employed in CO_2 concentration, heating rates, and sample composition.

3.5 Catalytic Evaluations

A blank experiment, conducted under previously described reactional conditions (Sect. 2.3., $CH_4/CO_2 = 1$), ensured the absence of non–catalytic gas phase reaction (negligible conversion). The experimental error was estimated to be about ± 2.2% (maximum), by analysis of variance (student t–test), conducted in triplicated evaluation (DRM at 800 ºC, $CH_4/CO_2 = 1$−sample Ni–WC carburized at 850 ºC). The results (Fig. 10) showed that Ni–WC carburized at 850 °C was active and relatively stable, during 20 h (time–on–stream), for any of the CH_4/CO_2 molar ratios employed (Tests 1, 2 and 3). On the other hand, Ni–Mo_2C carburized at 850 °C only showed activity and stability when CH_4/CO_2 molar ratio was higher or equal to 1 (Tests 1 and 2). Moreover, if employed a CH_4/CO_2 molar ratio less than 1 (Test 3) a rapid and intense deactivation occurred by oxidation of Mo_2C to MoO_2, as verified by XRD (Fig. 6).

During the catalytic tests using Ni–WC, when employed $CH_4/CO_2 \geq 1$ (Tests 1 and 2), there was a slight and progressive increase in gauge pressure tending to stabilizes near 1.5 bar at the end of analyzed period. This behavior corroborates the observed tendency of carbon deposition, also evidenced by XRD results of the catalysts after reaction (Fig. 6), which could lead to their deactivation when utilized for long periods. The NiMo sample, in turn, did not present a significant increase in pressure for any of the performed tests. Furthermore, no graphite carbon was detected by XRD of this sample after the reaction.

Thermodynamic calculations of DRM showed, for $CH_4/CO_2 = 1$ at atmospheric pressure and 800 °C, the CH_4 equilibrium conversion ($X^{eq}_{CH_4} = 96.3\%$) is higher than CO_2 equilibrium conversion ($X^{eq}_{CO_2} = 88.6\%$) and H_2/CO ratio is equal to 1.1 [16]. However, analyzing results in Fig. 10 for $CH_4/CO_2 = 1$, we could observe that Ni–Mo_2C catalyst yielded a CO_2 conversion ($X_{CO2} \cong 80\%$) higher than CH_4 conversion ($X_{CH4} \cong 65\%$) and an H_2/CO ratio close to 0.75. Ni–WC presented a similar trend, CO_2 conversion ($X_{CO2} \cong 85\%$) higher than CH_4 conversion ($X_{CH4} \cong 75\%$) and an H_2/CO ratio nearly 0.77, also in this case lower

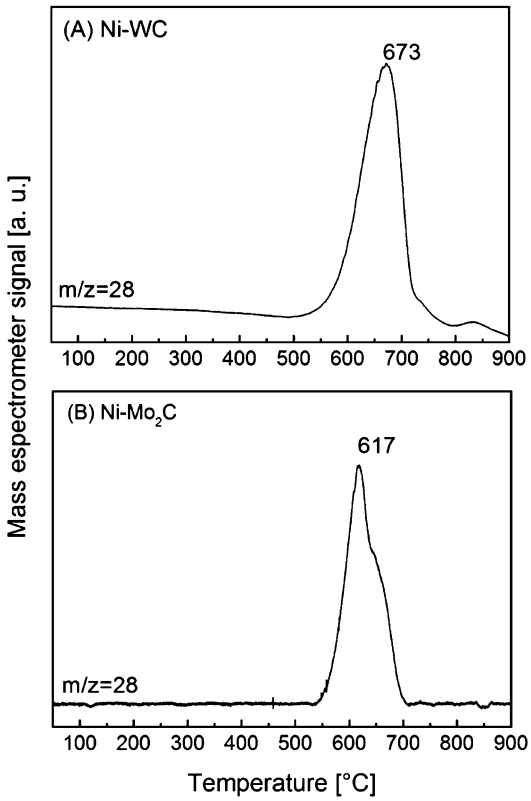

Fig. 9 CO_2/He–TPO profiles: (**a**) Ni–WC and (**b**) Ni–Mo_2C (carburized at 850 ºC)

than the calculated. The observed higher conversion of CO_2 can be explained by the occurrence of the following reactions: Reverse Boudouard reaction ($CO_2 + C_{(S)} \rightarrow 2$ CO), where CO_2 from the feed can gasify the carbon present on the catalyst; CO_2 activation on the carbides ($CO_2 \rightarrow CO + O^*$) that could lead to the carbide oxidation ($M_2C + 5O^* \rightarrow 2\,MO_2 + CO$, $MC + 3O^* \rightarrow MO_2 + CO$, where M = Mo or W); Reverse water–gas–shift (RWGS) ($CO_2 + H_2 \rightarrow CO + H_2O$) where, part of the produced H_2 is consumed (decreasing the H_2/CO ratio and H_2 yield) by reaction with CO_2, increasing its conversion. Furthermore, under the employed conditions, the RWGS reaction occurs in the gas phase, regardless of the presence or nature of the catalyst, and should be considered at thermodynamic equilibrium [30].

Darujati et al. (2003), employing bulk Mo_2C in DRM, proposed that the catalyst only was stable if the so–called stability ratio ($R_S = \frac{P_{H2}+P_{CO}}{P_{CO2}+P_{H2O}}$) exhibit value greater than 0.8 [47]. Thus, the fast deactivation of Ni–Mo_2C when CH_4/CO_2 was around 0.67 can be explained by considering that the increase in the CO_2 partial pressure in reaction mixture leads to a decrease in stability ratio (R_S) to values below 0.8. This effect also explains the decrease of W_2C phase diffraction intensity in the NiW catalyst (Fig. 6.a) with CH_4/CO_2 ratio around 0.67.

According to results in present work and similar studies published in the literature, Ni–Mo_2C and Ni–WC may be considered bifunctional catalysts. The stability of these catalysts may be associated to a continuous cycle of oxidation/(re)carburization where Mo_2C, W_2C, and WC carbides are more favorable to promote the activation of CO_2 ($CO_2 \rightarrow CO + O^*$) leading to their oxidation ($M_2C + 5O^* \rightarrow 2MO_2 + CO$, $MC + 3O^* \rightarrow MO_2 + CO$, where M = Mo or W), whereas metallic nickel (Ni^0) is more suitable to promote CH_4 decomposition ($CH_4 \rightarrow C^* + 2H_2$) and (re)carburization of the oxides by pyrolytic carbon ($2MO_2 + 5C^* \rightarrow M_2C + 4CO$, $MO_2 + 3C^* \rightarrow MC + 2CO$, where M = Mo or W). The ability of molybdenum and tungsten carbides to act as redox catalysts in DRM is previously reported in the literature [3, 15, 46, 48, 49].

The results of CH_4/He–TPC for the catalysts precursors (Fig. 8) together with the results of CO_2/He–TPO for the carburized catalysts (Fig. 9) corroborate with the hypothesis initially pointed out of oxidation/(re)carburization cycles during the DRM reaction.

Based on the results shown in Figs. 6–10, it can be pointed out that oxidation rates should be equal to (re)carburization rates to keep the catalyst stability over a continuous cycle of oxidation/(re)carburization. Furthermore, the Ni–Mo_2C catalyst is stable with $CH_4/CO_2 \geq 1$, assuming the carbide oxidation rate equal to the MoO_2 re-loading rate in the catalyst.

Similarly, the carbon formation in the Ni–WC catalyst is more intense because WC is more stable and less susceptible to the oxidation/(re)carburization cycle. In summary, the Ni–WC catalyst proved to be stable only with an excess of CO_2, which contributes to the effective removal of carbon formed at nickel sites; This carbon formation was detectable by XRD and Raman analysis (Figs. 6 and 7).

4 Conclusion

Ni–WC and Ni–Mo_2C were active catalysts in dry reforming of methane at atmospheric pressure and temperature of 800 ºC. However, their stability proved to be sensitive to the variation of CH_4/CO_2 molar ratio. Ni–Mo_2C was stable under $CH_4/CO_2 \geq 1$, whereas Ni–WC was stable when $CH_4/CO_2 < 1$. Thus, the cause of deactivation of these catalysts was due to the oxidation of the carbidic phase (Mo_2C–Mo_xO_y), when $CH_4/CO_2 < 1$; or by carbon deposition on Ni–WC for $CH_4/CO_2 \geq 1$. The activity of these catalysts, admitted bifunctional, was related to the oxidation/(re) carburization cycles. Mo_2C may be oxidized by CO_2 at lower temperatrures than WC. In the same way, molybdenum oxide

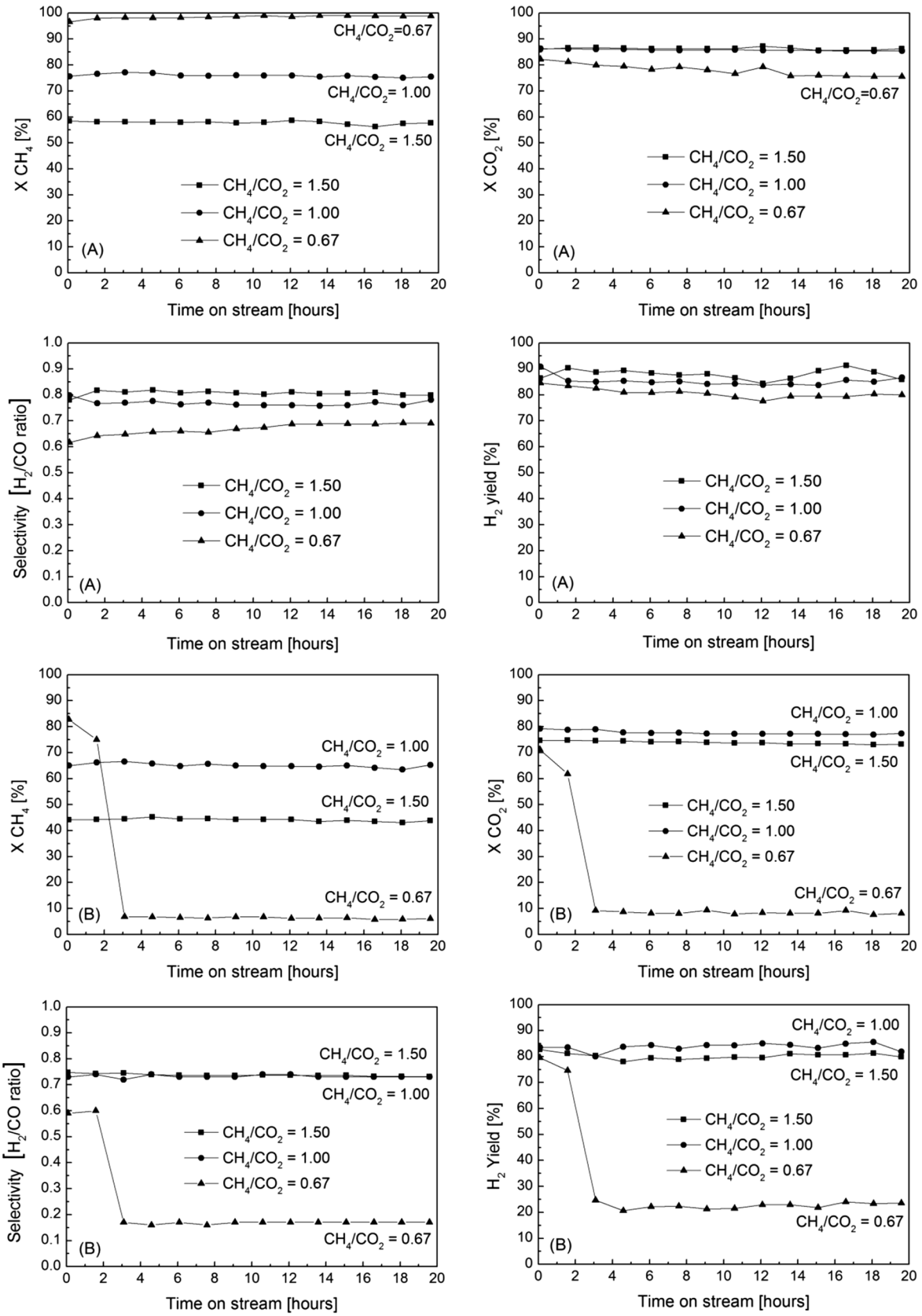

Fig. 10 DRM performance at variated ratio of CH_4/CO_2 (1.50, 1.00, 0.67) (T = 800 ºC, P = 1 atm): (**a**) Ni–WC; (**b**) Ni–Mo_2C

(Mo_xO_y) is more easily carburized than tungsten oxide (W_xO_y).

Pyrolytic carbon deposited over nickel metal sites played a fundamental role in maintaining the Ni–Mo_2C and Ni–WC catalyst activity, despite being the main cause of deactivation of conventional catalysts. In this case, carbon, as graphite, was responsible for the carbothermic (re)carburization of the molybdenum or tungsten oxy–carbides that had been partially oxidized by CO_2.

Acknowledgments The authors thank for the financial support provided by CNPq, CAPES, and PETROBRAS. We would like to dedicate this work to the memory of Prof. Victor Teixeira da Silva.

References

1. York APE, Claridge JB, Brungs AJ et al (1997) Molybdenum and tungsten carbides as catalysts for the conversion of methane to synthesis gas using stoichiometric feedstocks. Chem Commun. https://doi.org/10.1039/a605693h
2. York APE, Claridge JB, Márquez-Alvarez C et al (1997) Synthesis of early transition metal carbides and their application for the reforming of methane to synthesis gas. Stud Surf Sci Catal 110:711–720. https://doi.org/10.1016/S0167-2991(97)81033-6
3. Claridge JB, York APE, Brungs AJ et al (1998) New catalysts for the conversion of methane to synthesis gas: molybdenum and tungsten carbide. J Catal 180:85–100. https://doi.org/10.1006/jcat.1998.2260
4. British petroleum (2018) Statistical Review of World Energy 2018
5. Iyer MV, Norcio LP, Kugler EL, Dadyburjor DB (2003) Kinetic Modeling for Methane Reforming with Carbon Dioxide over a Mixed-Metal Carbide Catalyst. Ind Eng Chem Res 42:2712–2721. https://doi.org/10.1021/ie020677q
6. UFRJ–IBP (2017) Gás do Pré-Sal Oportunidades Desafios e Perspectivas. In: Colomer M (ed) Ciclo de Debates sobre Petróleo e Economia. Instituto Brasileiro de Petróleo e Gás, Rio de Janeiro, p 46
7. Rochedo PRR, Costa IVL, Império M et al (2016) Carbon capture potential and costs in Brazil. J Clean Prod 131:280–295. https://doi.org/10.1016/j.jclepro.2016.05.033
8. Teixeira da Silva VLS (2016) Catalytic Dry Reforming of Methane over Ni/β-Mo2C Catalysts. In: The 11th Natural Gas Conversion Symposium. Tromso, Norway
9. Hanif A, Suhartanto T, Green MLH (2002) Possible Utilisation of CO2 on Natuna's Gas Field Using Dry Reforming of Methane to Syngas (CO & H2). In: SPE–Asia Pacific Oil and Gas Conference and Exhibition, Perth, Australia, 8-10. pp 833–840
10. Usman M, Wan Daud WMA, Abbas HF (2015) Dry reforming of methane: Influence of process parameters—a review. Renew Sustain Energy Rev 45:710–744. https://doi.org/10.1016/j.rser.2015.02.026
11. Shao H, Kugler EL, Ma W, Dadyburjor DB (2005) Effect of temperature on structure and performance of in-house cobalt-tungsten carbide catalyst for dry reforming of methane. Ind Eng Chem Res 44:4914–4921. https://doi.org/10.1021/ie049186r
12. Shao H, Kugler EL, Dadyburjor DB et al (2009) Correlating NEXAFS characterization of Co-W and Ni-W bimetallic carbide catalysts with reactivity for dry reforming of methane. Appl Catal A Gen 356:18–22. https://doi.org/10.1016/j.apcata.2008.11.012
13. Cheng J, Huang W (2010) Effect of cobalt (nickel) content on the catalytic performance of molybdenum carbides in dry-methane reforming. Fuel Process Technol 91:185–193. https://doi.org/10.1016/j.fuproc.2009.09.011
14. Arora S, Prasad R (2016) An overview on dry reforming of methane: strategies to reduce carbonaceous deactivation of catalysts. RSC Adv 6:108668–108688. https://doi.org/10.1039/C6RA20450C
15. Yao Z, Jiang J, Zhao Y et al (2016) Insights into the deactivation mechanism of metal carbide catalysts for dry reforming of methane via comparison of nickel-modified molybdenum and tungsten carbides. RSC Adv 6:19944–19951. https://doi.org/10.1039/C5RA24815A
16. Nikoo MK, Amin NAS (2011) Thermodynamic analysis of carbon dioxide reforming of methane in view of solid carbon formation. Fuel Process Technol 92:678–691. https://doi.org/10.1016/j.fuproc.2010.11.027
17. Iyer MV, Norcio LP, Punnoose A et al (2004) Catalysis for synthesis gas formation from reforming of methane. Top Catal 29:197–200. https://doi.org/10.1023/B:TOCA.0000029803.90815.68
18. de Oliveira PMCR (2016) Carbeto de molibdenio promovido por niquel como catalisador na reforma seca de metano. UFRJ/COPPE, Rio de Janeiro
19. Li Y, Wang Y, Zhang X, Mi Z (2008) Thermodynamic analysis of autothermal steam and CO2 reforming of methane. Int J Hydrogen Energy 33:2507–2514. https://doi.org/10.1016/j.ijhydene.2008.02.051
20. Zou H, Chen S, Huang J, Zhao Z (2016) Effect of additives on the properties of nickel molybdenum carbides for the tri-reforming of methane. Int J Hydrogen Energy 41:16842–16850. https://doi.org/10.1016/j.ijhydene.2016.07.108
21. Bradford MCJ, Vannice MA (1996) Catalytic reforming of methane with carbon dioxide over nickel catalysts II. Reaction kinetics Appl Catal A Gen 142:97–122. https://doi.org/10.1016/0926-860X(96)00066-X
22. Korobitsyn M, Berkel F Van, Christie G (2000) SOFC as a gas separator–Final Report
23. Bradford MCJ, Vannice MA (1998) CO2 reforming of CH4 over supported Pt catalysts. J Catal 173:157–171. https://doi.org/10.1006/jcat.1997.1910
24. Teuner SC, Neumann P, Von Linde F (2001) CO through CO2 reforming –the Calcor standard and Calcor economy processes. Oil Gas Eur Mag 27:44–46
25. Gunardson H (1998) Industrial gases in petrochemical processing. CRC Press, New York, NY
26. Maroto-Valer MM, Song C, Soong Y (2002) Environmental challenges and greenhouse gas control for fossil fuel utilization in the 21st century. Kluwer Academic / Plenum Publishers, San Diedo, California
27. Pienkowski L, Motak M, Dabek R, Jaszczur M (2018) Use of HTGR process heat with catalysts for dry reforming of methane using CO2 to singas for the chemical industry, AGH
28. Shamsi A (2002) Methane dry reforming over carbide, nickel-based, and noble metal catalysts. In: Song C, Gaffney AF, Fujimoto K (eds) ACS symposium series. American Chemical Society, Washington, DC, pp 182–196
29. Pakhare D, Spivey J (2014) A review of dry (CO 2) reforming of methane over noble metal catalysts. Chem Soc Rev 43:7813–7837. https://doi.org/10.1039/C3CS60395D
30. Silva CG, Passos FB, da Silva VT (2019) Influence of the support on the activity of a supported nickel-promoted molybdenum carbide catalyst for dry reforming of methane. J Catal 375:507–518. https://doi.org/10.1016/j.jcat.2019.05.024
31. Armor JN (1999) The multiple roles for catalysis in the production of H2. Appl Catal A Gen 176:159–176. https://doi.org/10.1016/S0926-860X(98)00244-0
32. Pritchard ML, McCauley RL, Gallaher BN, Thomson WJ (2004) The effects of sulfur and oxygen on the catalytic activity of

molybdenum carbide during dry methane reforming. Appl Catal A Gen 275:213–220. https://doi.org/10.1016/j.apcata.2004.07.035
33. Gaillard M, Virginie M, Khodakov AY (2017) New molybdenum-based catalysts for dry reforming of methane in presence of sulfur: A promising way for biogas valorization. Catal Today 289:143–150. https://doi.org/10.1016/j.cattod.2016.10.005
34. Oyama ST (1992) Preparation and catalytic properties of transition metal carbides and nitrides. Catal Today 15:179–200. https://doi.org/10.1016/0920-5861(92)80175-M
35. Koverga AA, Flórez E, Dorkis L, Rodriguez JA (2020) Promoting effect of tungsten carbide on the catalytic activity of Cu for CO2 reduction. Phys Chem Chem Phys 22:13666–13679. https://doi.org/10.1039/D0CP00358A
36. Prats H, Gutiérrez RA, Piñero JJ et al (2019) Room temperature methane capture and activation by Ni clusters supported on TiC(001): effects of metal-carbide interactions on the cleavage of the C–H Bond. J Am Chem Soc 141:5303–5313. https://doi.org/10.1021/jacs.8b13552
37. Hall DS, Lockwood DJ, Bock C et al (2015) Nickel hydroxides and related materials: a review of their structures, synthesis and properties. Proceedings Math Phys Eng Sci. https://doi.org/10.1098/rspa.2014.0792
38. Thommes M, Kaneko K, Neimark AV et al (2015) Physisorption of gases, with special reference to the evaluation of surface area and pore size distribution (IUPAC Technical Report). Pure Appl Chem 87:1051–1069. https://doi.org/10.1515/pac-2014-1117
39. Resini C, Montanari T, Barattini L et al (2009) Hydrogen production by ethanol steam reforming over Ni catalysts derived from hydrotalcite-like precursors: Catalyst characterization, catalytic activity and reaction path. Appl Catal A Gen 355:83–93. https://doi.org/10.1016/j.apcata.2008.11.029
40. Oliva P, Leonardi J, Laurent JF et al (1982) Review of the structure and the electrochemistry of nickel hydroxides and oxy-hydroxides. J Power Sources 8:229–255. https://doi.org/10.1016/0378-7753(82)80057-8
41. Levin D, Soled SL, Ying JY (1996) Crystal structure of an ammonium nickel molybdate prepared by chemical precipitation. Inorg Chem 35:4191–4197. https://doi.org/10.1021/ic951200s
42. Rives V, Angeles Ulibarri M (1999) Layered double hydroxides (LDH) intercalated with metal coordination compounds and oxometalates. Coord Chem Rev 181:61–120. https://doi.org/10.1016/S0010-8545(98)00216-1
43. Xiao T, Wang H, York APE et al (2002) Preparation of nickel-tungsten bimetallic carbide catalysts. J Catal 209:318–330. https://doi.org/10.1006/jcat.2002.3651
44. Lee J (1987) Molybdenum carbide catalysts I. Synthesis of unsupported powders. J Catal 106:125–133. https://doi.org/10.1016/0021-9517(87)90218-1
45. Lobo AO, Martin AA, Antunes EF et al (2005) Caracterização de materiais carbonosos por espectroscopia Raman. Rev Bras Apl Vácuo 24:98–103. https://doi.org/10.17563/rbav.v24i2.99
46. Shi C, Zhang A, Li X et al (2012) Ni-modified Mo2C catalysts for methane dry reforming. Appl Catal A Gen 431–432:164–170. https://doi.org/10.1016/j.apcata.2012.04.035
47. LaMont DC, Gilligan AJ, Darujati ARS et al (2003) The effect of Mo2C synthesis and pretreatment on catalytic stability in oxidative reforming environments. Appl Catal A Gen 255:239–253. https://doi.org/10.1016/S0926-860X(03)00567-2
48. Guo J, Zhang AJ, Zhu AM et al (2010) A carbide catalyst effective for the dry reforming of methane at atmospheric pressure. In: Hu YH (ed) ACS symposium series. American Chemical Society.pp, Washington, DC, pp 181–196
49. Gao H, Yao Z, Shi Y, Wang S (2018) Improvement of the catalytic stability of molybdenum carbide via encapsulation within carbon nanotubes in dry methane reforming. Catal Sci Technol 8:697–701. https://doi.org/10.1039/c7cy02506h